

Analytical study of flow and heat transfer in an annular porous medium subject to asymmetrical heat fluxes

Huijin Xu^{1,2,3} · Changying Zhao² · Kambiz Vafai³

Received: 27 August 2016 / Accepted: 3 March 2017 / Published online: 14 March 2017
© Springer-Verlag Berlin Heidelberg 2017

Abstract Fully developed forced convective heat transfer in an annulus filled with a porous medium subject to asymmetrical heating is investigated analytically with different models in this work. The classic Darcy and Brinkman models were employed for the fluid flow, while the local thermal equilibrium (LTE) and the local thermal non-equilibrium (LTNE) models were employed to describe the heat transfer process in porous media. An analytical model based on fin theory was also employed for analyzing this problem. Exact solutions with Darcy-LTNE, Darcy-LTE, Brinkman-LTNE, Brinkman-LTE, and the fin models were obtained. Among these solutions, the Brinkman-LTNE solution can be treated as the benchmark, as it is a complete model, which covers the effect of viscous force near the solid wall and the temperature difference between the solid and fluid phases. The basic parameters that affect the velocity and temperature fields were analyzed in depth. The velocity and temperature profiles with these different models were also presented. The effects of some critical parameters on thermal performance of asymmetrically heated annulus fitted with a porous medium were discussed. The cited different analytical models were compared in detail with each other. The critical heat flux (HF) ratios for the inner and outer walls were presented in terms of a $Nu-\xi$ curve for the five models. These solutions

were developed for an asymmetrically heated annular channel filled with a porous medium, which can predict the thermal performance within a wide range of radii and HF ratios.

List of symbols

a_{sf}	Specific surface area (m^{-1})
A	Area (m^2)
c_p	Specific heat ($J\ kg^{-1}\ K^{-1}$)
Da	Darcy number
f	Friction factor
h	Heat transfer coefficient ($W\ m^{-2}\ K^{-1}$)
h_{sf}	Local convective heat transfer coefficient ($W\ m^{-2}\ K^{-1}$)
K	Permeability (m^2)
k	Thermal conductivity ($W\ m^{-1}\ K^{-1}$)
k_r	Thermal conductivity ratio ($k_r = k_f/k_s$)
M	Viscosity ratio
Nu	Nusselt number
p	Pressure ($N\ m^{-2}$)
P	Dimensionless pressure drop
Pr	Prandtl number
q	Heat flux ($W\ m^{-2}$)
r	Radius (m)
r_1	Inner radius (m)
r_2	Outer radius (m)
R	Dimensionless radius
R_2	Radius ratio
Re	Reynolds number
s	Shape factor
t	Dimensionless factor
T	Temperature (K)
u	Velocity ($m\ s^{-1}$)
u_m	Mean velocity ($m\ s^{-1}$)
U	Dimensionless velocity
x	Axial position (m)

✉ Kambiz Vafai
vafai@engr.ucr.edu

¹ Department of Energy and Power Engineering, College of Pipeline and Civil Engineering, China University of Petroleum, Qingdao 266580, China

² Institute of Engineering Thermophysics, Shanghai Jiao Tong University, Shanghai 200240, China

³ Department of Mechanical Engineering, University of California, Riverside, CA 92521, USA

Greek symbols

ε	Porosity
θ	Dimensionless temperature
μ	Dynamic viscosity ($\text{kg m}^{-1} \text{s}^{-1}$)
ξ	Heat flux ratio
ρ	Density (kg m^{-3})
φ	Polar angle (rad)

Subscripts

1	Inner wall
2	Outer wall
b	Bulk
e	Effective
f	Fluid
fe	Effective value of fluid
i	Interface
m	Mean
p	Porous
r	Ratio
s	Solid
se	Effective value of solid
w	Wall

1 Introduction

Transport in porous media has been continuously receiving increased attention for the past decades. This stems from its critical importance in many engineering areas, such as oil extraction [1], heat transfer enhancement [2], solar thermal utilization [3], electronics cooling [4], thermal storage [5], chemical reforming [6], modeling of biological tissues [7], as well as many other areas. Another area of interest is the highly conductive porous media, such as metallic/carbon foams with open cells [8], sintered metallic fiber felts [9], packed beds [10], metallic lattice frame structures [11], which facilitates the vast applications of porous media in industry.

The volume averaging technique is a commonly used method for handling transport in porous structures [12]. The Darcy, Brinkman, and Forchheimer models have been used in various research works. The Brinkman model accounts for the viscous effect of an impermeable wall, while the Forchheimer model with quadratic term is appropriate for high velocity flows. For thermal transport in porous media, either local thermal equilibrium (LTE) or local thermal non-equilibrium (LTNE) models are utilized.

For steady convective heat transfer, when the difference between the thermal conductivity of the fluid phase and that of the solid phase is small, the LTE model is an efficient tool for predicting the heat transfer in porous media. Cheng and Hsu [13] numerically studied the fully-developed, forced convective flow and heat transfer through packed bed of spheres in an annular space with Brinkman

and LTE models by considering the effects of porosity and permeability variations near the wall. Vafai and Tien [14] performed a theoretical study for moisture transport of fluid in porous materials and the coupling heat/mass transfer process was numerically simulated based on LTE model. Chikh et al. [15] analytically investigated the forced convective heat transfer in an annulus partially filled with a porous medium subject to a constant heat flux, and analyzed the effect of the porous layer thickness on the Nusselt number. Mitrovic and Maletic [16] numerically solved the forced convective heat transfer in a porous annulus with asymmetrical thermal boundary conditions for the inner and outer walls. Mitrovic and Maletic [17] presented a numerical analysis for laminar forced convective heat transfer in a parallel-plate channel filled with a porous medium subject to asymmetrical thermal boundary conditions using the LTE model. Cekmer et al. [18] presented an analytical solution for forced convection in a parallel-plate channel filled with a porous medium when exposed to asymmetrical wall heat fluxes by using LTE model, and analyzed the effect of heat flux ratio on the heat transfer.

LTNE model has received much attention for handling thermal problems in porous media. The importance of using LTNE model was comprehensively established and analyzed in the papers by Vafai and Sozen [19, 20], and Sozen and Vafai [21, 22]. Kuznetsov [23] presented a perturbation solution of heat transfer in a concentric annulus with Darcy model and LTNE model. Lee and Vafai [24] presented a comprehensive analytical study of convective heat transfer in a parallel-plate channel filled with porous media, and presented the parametric analysis for the thermal performance, while analyzing various aspects of the LTNE model. Xu et al. [25] analyzed the LTNE phenomena in metal-foam channel and found there are two main factors affecting thermal transport in porous media: porosity and thermal conductivity ratio of fluid to solid (k_p). Using the Brinkman flow model and the LTNE model, Lu et al. [26] presented an analytical solution for forced convection in a tube filled with porous foams, and Zhao et al. [27] presented the analytical solution for forced convection in an annulus filled with porous foams. Shaikh and Memon [28] provided analytical and numerical solutions for forced convective heat transfer in a circular duct with or without porous medium using Darcy–Brinkman–Forchheimer model. Ouyang et al. [29] performed an analytical investigation on developing forced convective heat transfer in a parallel-plate channel filled with a porous medium. Yang and Vafai [30] utilized a comprehensive analysis of the boundary conditions to present an analytical solution for forced convective heat transfer in a porous medium channel and for the first time established the presence of temperature bifurcation in porous media. Xu et al. [31] developed an explicit analytical solution for Brinkman flow and

non-equilibrium heat transfer in a parallel-plate channel filled with micro-foams under the condition of asymmetric heat fluxes, and analyzed the effect of basic parameters on Nusselt numbers at the two walls.

Amongst these publications, Refs. [13, 15, 16, 23] consider the forced convection in annular configurations, and Refs. [16–18, 31] address the asymmetrical thermal boundary conditions. Tubular configurations with annular space are extensively utilized in industrial applications, such as heat exchangers, solar collectors, chemical reactors, heat accumulators, heat pipes, and electronic heat sinks. Thermal asymmetrical heating is frequently encountered in these applications. As such an analytical investigation of the non-equilibrium heat transfer in an annular space filled with a porous medium under asymmetrical thermal boundary conditions is very important.

To this end, we will employ the LTNE model to obtain analytical solutions for forced convection in an annular duct filled with a porous material subject to a thermally asymmetrical condition. The Darcy and Brinkman models will be used with LTE and LTNE models, and the fin-theory-based model will also be utilized. The effects of key parameters on different models will be analyzed in depth.

2 Physical problem

The schematic diagram of forced convective heat transfer in a concentric annulus is shown in Fig. 1. The annulus is filled with a porous medium. The radius of the inner wall is r_1 and that of the outer wall is r_2 . Different heat fluxes are imposed on the inner and outer walls. The following commonly used assumptions are imposed: (1) porous medium which fills the annulus is both homogeneous and isotropic; (2) thermophysical properties of the fluid and porous

medium are independent of the temperature; (3) hydraulically and thermally fully developed conditions are considered and the fluid is taken to be Newtonian.

3 Analysis

For thermally and hydraulically fully developed forced convection, the following conditions can be imposed:

$$\begin{aligned} \frac{\partial u}{\partial x} = 0, \quad v = 0, \quad \frac{\partial p}{\partial r} = 0, \quad \frac{dp}{dx} = \text{const}, \quad h_{1x} = \text{const}, \quad h_{2x} = \text{const}, \\ \frac{\partial T_f}{\partial x} = \frac{\partial T_s}{\partial x} = \frac{dT_{f,b}}{dx} = \frac{dT_{w1}}{dx} = \frac{dT_{w2}}{dx} = \text{const} \end{aligned} \quad (1)$$

The governing equations of the present problem with Brinkman term and LTNE model can be referred from Ref. [19]. The simplified momentum equation with the Brinkman term is

$$0 = -\frac{dp}{dx} + \mu_e \frac{1}{r} \frac{\partial}{\partial r} \left(r \frac{\partial u}{\partial r} \right) - \frac{\mu_f}{K} u \quad (2)$$

For the LTE model, the difference between solid and fluid temperatures is neglected. The energy equation can be presented by

$$\rho_f c_f u \frac{\partial T_f}{\partial x} = k_e \frac{1}{r} \frac{\partial}{\partial r} \left(r \frac{\partial T_f}{\partial r} \right) \quad (3)$$

While, under LTNE condition, the solid and fluid energy equations are as follows:

$$\begin{cases} \text{solid :} & 0 = k_{se} \frac{1}{r} \frac{\partial}{\partial r} \left(r \frac{\partial T_s}{\partial r} \right) - h_{sf} a_{sf} (T_s - T_f) \\ \text{fluid :} & \rho_f c_f u \frac{\partial T_f}{\partial x} = k_{fe} \frac{1}{r} \frac{\partial}{\partial r} \left(r \frac{\partial T_f}{\partial r} \right) + h_{sf} a_{sf} (T_s - T_f) \end{cases} \quad (4)$$

The corresponding boundary conditions are

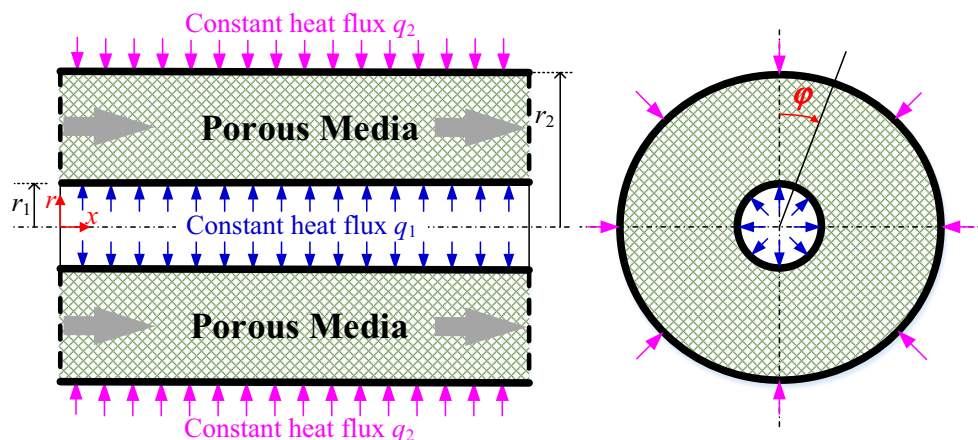


Fig. 1 Schematic diagram of the problem under consideration

$$\begin{cases} r = r_1 : & u = 0, T_s = T_f = T_{w1}, k_{se} \frac{\partial T_s}{\partial r} + k_{fe} \frac{\partial T_f}{\partial r} = -q_1 \\ r = r_2 : & u = 0, T_s = T_f = T_{w2}, k_{se} \frac{\partial T_s}{\partial r} + k_{fe} \frac{\partial T_f}{\partial r} = q_2 \end{cases} \quad (5)$$

In obtaining the analytical solutions, the following dimensionless parameters are employed.

$$\begin{aligned} R &= \frac{r}{r_1}, U = \frac{u}{u_m}, Da = \frac{K}{r_1^2}, P = \frac{K}{\mu_f u_m} \frac{dp}{dx}, \\ M &= \frac{\mu_e}{\mu_f}, s = \sqrt{\frac{1}{M \cdot Da}} \\ \theta_{s(f)} &= \frac{T_{s(f)} - T_{w1}}{q_2 \cdot r_1 / k_{se}}, B = \frac{k_f}{k_{se}}, \\ C &= \frac{k_{fe}}{k_{se}}, D = \frac{h_{sf} a_{sf} r_1^2}{k_{se}}, \xi = \frac{q_1}{q_2}, t = \sqrt{\frac{D(C+1)}{C}} \end{aligned} \quad (6)$$

3.1 Darcy-LTNE model

In the Darcy flow model, the velocity distribution at the cross-section is uniform. The governing equations for the solid and fluid phases are normalized as

$$\begin{cases} \text{solid} : & 0 = \frac{1}{R} \frac{\partial}{\partial R} \left(R \frac{\partial \theta_s}{\partial R} \right) - D(\theta_s - \theta_f) \\ \text{fluid} : & \frac{2(\xi + R_2)}{R_2^2 - 1} = C \frac{1}{R} \frac{\partial}{\partial R} \left(R \frac{\partial \theta_f}{\partial R} \right) + D(\theta_s - \theta_f) \end{cases} \quad (7)$$

The dimensionless boundary conditions are

$$\begin{cases} R = 1 : & \theta_s = \theta_f = 0, \frac{\partial \theta_s}{\partial R} + C \frac{\partial \theta_f}{\partial R} = -\xi \\ R = R_2 : & \theta_s = \theta_f = \theta_{w2}, \frac{\partial \theta_s}{\partial R} + C \frac{\partial \theta_f}{\partial R} = 1 \end{cases} \quad (8)$$

The solid and fluid temperature distributions can be obtained analytically as

$$\theta_s = \frac{2(\xi + R_2)}{R_2^2 - 1} \left\{ A_3 I_0(tR) + A_4 K_0(tR) + \frac{1}{4(C+1)} R^2 + \frac{A_1}{C+1} \ln(R) + \frac{A_2}{C+1} + \frac{C}{D(C+1)^2} \right\} \quad (9a)$$

$$\theta_f = \frac{2(\xi + R_2)}{R_2^2 - 1} \left\{ -\frac{1}{C} [A_3 I_0(tR) + A_4 K_0(tR)] + \frac{1}{4(C+1)} R^2 + \frac{A_1}{C+1} \ln(R) + \frac{A_2}{C+1} - \frac{1}{D(C+1)^2} \right\} \quad (9b)$$

where the constants A_1, A_2, A_3 and A_4 are as follows

$$\begin{aligned} A_1 &= \frac{R_2^3 - R_2}{2(\xi + R_2)} - \frac{R_2^2}{2} \\ A_2 &= -\frac{1}{4} \\ A_3 &= -\frac{K_0(tR_2) - K_0(t)}{I_0(t)K_0(tR_2) - K_0(t)I_0(tR_2)} \cdot \frac{C}{D(C+1)^2} \\ A_4 &= -\frac{I_0(tR_2) - I_0(t)}{K_0(t)I_0(tR_2) - I_0(t)K_0(tR_2)} \cdot \frac{C}{D(C+1)^2} \end{aligned} \quad (10)$$

3.2 Darcy-LTE model

For the Darcy model of flow through a porous medium, the effect of impermeable wall on the flow is neglected, and the velocity distribution at a given cross-section is considered to be uniform. In this case, for fully-developed forced convection, the dimensionless energy equation for the LTE model is

$$\frac{1}{R} \frac{\partial}{\partial R} \left(R \frac{\partial \theta_f}{\partial R} \right) = \frac{2(\xi + R_2)}{(C+1)(R_2^2 - 1)} \quad (11)$$

The dimensionless closure conditions can be represented by

$$\begin{cases} R = 1 : & \theta_f = 0 \\ R = R_2 : & (C+1) \frac{\partial \theta_f}{\partial R} = 1 \end{cases} \quad (12)$$

The analytical solution for the Darcy-LTE model is obtained as

$$\begin{aligned} \theta_f &= \frac{2(\xi + R_2)}{(C+1)(R_2^2 - 1)} \left\{ \frac{1}{4} (R^2 - 1) + \left[\frac{R_2(R_2^2 - 1)}{2(\xi + R_2)} - \frac{R_2^2}{2} \right] \cdot \ln(R) \right\} \end{aligned} \quad (13)$$

3.3 Brinkman-LTNE model

With the LTNE model, the dimensionless equations for flow and heat transfer are

$$\begin{cases} \text{momentum eq.} : & 0 = \frac{1}{R} \frac{\partial}{\partial R} \left(R \frac{\partial U}{\partial R} \right) - s^2(U + P) \\ \text{solid energy eq.} : & 0 = \frac{1}{R} \frac{\partial}{\partial R} \left(R \frac{\partial \theta_s}{\partial R} \right) - D(\theta_s - \theta_f) \\ \text{fluid energy eq.} : & \frac{2(\xi + R_2)}{R_2^2 - 1} U = C \frac{1}{R} \frac{\partial}{\partial R} \left(R \frac{\partial \theta_f}{\partial R} \right) + D(\theta_s - \theta_f) \end{cases} \quad (14)$$

The dimensionless boundary conditions are

$$\begin{cases} R = 1 : & U = 0, \theta_s = \theta_f = 0, \frac{\partial \theta_s}{\partial R} + C \frac{\partial \theta_f}{\partial R} = -\xi \\ R = R_2 : & U = 0, \theta_s = \theta_f = \theta_{w2}, \frac{\partial \theta_s}{\partial R} + C \frac{\partial \theta_f}{\partial R} = 1 \end{cases} \quad (15)$$

The analytical expression for the velocity is obtained as

$$U = P[C_1 I_0(sR) + C_2 K_0(sR) - 1] \quad (16)$$

where constants $C_1, C_2,$ and P are as follows

$$\begin{aligned} C_1 &= \frac{K_0(s) - K_0(sR_2)}{K_0(s) \cdot I_0(sR_2) - I_0(s) \cdot K_0(sR_2)} \\ C_2 &= \frac{I_0(s) - I_0(sR_2)}{I_0(s) \cdot K_0(sR_2) - K_0(s) \cdot I_0(sR_2)} \\ P &= \frac{1}{\frac{2[C_1[R_2 \cdot I_1(sR_2) - I_1(s)] - C_2[R_2 \cdot K_1(sR_2) - K_1(s)]]}{s(R_2^2 - 1)} - 1} \end{aligned} \quad (17)$$

The analytical solutions for temperatures of solid and fluid are obtained as follows

$$\theta_s = \frac{2(\xi + R_2)P}{R_2^2 - 1} \left\{ \begin{aligned} &C_5 I_0(tR) + C_6 K_0(tR) - \frac{\frac{D}{Cs^2}}{s^2 - \frac{D(C+1)}{C}} [C_1 I_0(sR) + C_2 K_0(sR)] \\ &-\frac{1}{4(C+1)} R^2 + \frac{C_3}{C+1} \ln(R) + \frac{C_4}{C+1} - \frac{C}{D(C+1)^2} \end{aligned} \right\} \tag{18a}$$

$$\theta_f = \frac{2(\xi + R_2)P}{R_2^2 - 1} \left\{ \begin{aligned} &-\frac{1}{C} [C_5 I_0(tR) + C_6 K_0(tR)] + \frac{1 - \frac{D}{s^2}}{C \left[s^2 - \frac{D(C+1)}{C} \right]} [C_1 I_0(sR) + C_2 K_0(sR)] \\ &-\frac{1}{4(C+1)} R^2 + \frac{C_3}{C+1} \ln(R) + \frac{C_4}{C+1} + \frac{C}{D(C+1)^2} \end{aligned} \right\} \tag{18b}$$

where the constant parameters C_3, C_4, C_5 and C_6 in the above equations are

$$\begin{aligned} C_3 &= \frac{R_2(R_2^2-1)}{2(\xi+R_2)P} - \frac{R_2}{s} [C_1 I_1(sR_2) - C_2 K_1(sR_2)] + \frac{R_2^2}{2} \\ C_4 &= \frac{1}{4} - \frac{1}{s^2} \\ C_5 &= \frac{K_0(t) - K_0(tR_2)}{K_0(t) \cdot I_0(tR_2) - I_0(t) \cdot K_0(tR_2)} \left[\frac{Cs^2}{s^2 - \frac{D(C+1)}{C}} \right] \frac{Cs^2}{D(C+1)^2} \\ C_6 &= \frac{I_0(t) - I_0(tR_2)}{I_0(t) \cdot K_0(tR_2) - K_0(t) \cdot I_0(tR_2)} \left[\frac{Cs^2}{s^2 - \frac{D(C+1)}{C}} \right] \frac{Cs^2}{D(C+1)^2} \end{aligned} \tag{19}$$

3.4 Brinkman-LTE model

In this part, the Brinkman model for flow and LTE model for heat transfer are employed. The governing equations are

$$\begin{cases} \text{Momentum eq. : } \frac{1}{R} \frac{\partial}{\partial R} \left(R \frac{\partial U}{\partial R} \right) - s^2(U + P) = 0 \\ \text{Energy eq. : } \frac{1}{R} \frac{\partial}{\partial R} \left(R \frac{\partial \theta_f}{\partial R} \right) = \frac{2(\xi+R_2)}{(C+1)(R_2^2-1)} U \end{cases} \tag{20}$$

The dimensionless boundary conditions are

$$\begin{cases} R = 1 : & U = 0, \theta_f = 0 \\ R = R_2 : & U = 0, (C+1) \frac{\partial \theta_f}{\partial R} = 1 \end{cases} \tag{21}$$

The analytical solution for velocity will be the same as that given in the prior section. The temperature solution is derived as

$$\theta_f = \frac{2(\xi + R_2)P}{(C+1)(R_2^2 - 1)} \left\{ \begin{aligned} &\frac{1}{s^2} [C_1 I_0(sR) + C_2 K_0(sR)] \\ &-\frac{1}{4} R^2 + C_7 \ln(R) + C_8 \end{aligned} \right\} \tag{22}$$

where the constants C_7 and C_8 are

$$\begin{aligned} C_7 &= \frac{R_2^3 - R_2}{2(\xi+R_2)P} - \frac{R_2}{s} [C_1 I_1(sR_2) - C_2 K_1(sR_2)] + \frac{R_2^2}{2} \\ C_8 &= \frac{1}{4} - \frac{1}{s^2} \end{aligned} \tag{23}$$

3.5 Fin model

For a highly-conductive porous material, the fluid temperature at a cross-section can be approximated to be relatively uniform due to the dominant solid heat conduction. In this case, the thermal conductivity of the fluid does not play a major role. As such, the fin analysis method can be introduced to obtain an approximate solution. The fin model is an approximate tool for evaluating the heat transfer in porous medium. In the fin analysis method, the velocity and fluid temperature is assumed to be uniform, and the heat transfer between the fins and the fluid is usually treated as an equivalent heat source for the heat conduction in the solid. The Darcy flow is considered in the fin model, Darcy-LTE model and Darcy-LTNE model with the assumption of uniform distribution of velocity. In the Brinkman-LTE model and Brinkman-LTNE model, the non-uniform distribution of velocity is considered. The purpose of adopting Darcy model is to be able to compare with the full model so as to examine the effect of non-uniform velocity on heat transfer. For the present problem of forced convection in an asymmetrically heated porous medium, the heat conduction equation for a porous fins can be written as

$$k_{se} \frac{1}{r} \frac{\partial}{\partial r} \left(r \frac{\partial T_s}{\partial r} \right) - h_{sf} a_{sf} (T_s - T_{f,b}) = 0 \tag{24}$$

Subject to the following boundary conditions

$$\begin{cases} r = r_1 : & k_{se} \frac{\partial T_s}{\partial r} = -q_1 \\ r = r_2 : & k_{se} \frac{\partial T_s}{\partial r} = q_2 \end{cases} \tag{25}$$

From the energy conservation, the bulk fluid temperature can be obtained as

$$T_{f,b}(x) = T_{f,in} + \frac{2x(q_1 r_1 + q_2 r_2)}{c_f \rho_f u_m (r_2^2 - r_1^2)} \tag{26}$$

Equation (24) for the porous fin can be normalized as

$$\frac{1}{R} \frac{\partial}{\partial R} \left(R \frac{\partial \theta_s}{\partial R} \right) - D(\theta_s - \theta_{f,b}) = 0 \tag{27}$$

It should be noted that the dimensionless bulk fluid temperature $\theta_{f,b}$ is a quantity that should be determined in the present fin analysis method. The dimensionless boundary conditions are

$$\begin{cases} R = 1 : \theta_s = 0, \frac{\partial \theta_s}{\partial R} = -\xi, \theta_s = -\theta_{f,b} \\ R = R_2 : \frac{\partial \theta_s}{\partial R} = 1 \end{cases} \tag{28}$$

In the fin analysis method, the dimensionless bulk fluid temperature $\theta_{f,b}$ is obtained as

$$\theta_{f,b} = - \frac{[K_1(\sqrt{D}) + \xi K_1(\sqrt{DR_2})]I_0(\sqrt{D}) + [I_1(\sqrt{D}) + \xi I_1(\sqrt{DR_2})]K_0\sqrt{D}}{\sqrt{D}[K_1(\sqrt{D})I_1(\sqrt{DR_2}) - I_1(\sqrt{D})K_1(\sqrt{DR_2})]} \tag{29a}$$

The solid temperature can be solved using the above equation to obtain

$$\theta_s = \frac{[K_1(\sqrt{D}) + \xi K_1(\sqrt{DR_2})][I_0(\sqrt{DR}) - I_0(\sqrt{D})] + [I_1(\sqrt{D}) + \xi I_1(\sqrt{DR_2})][K_0(\sqrt{DR}) - K_0(\sqrt{D})]}{\sqrt{D}[K_1(\sqrt{D})I_1(\sqrt{DR_2}) - I_1(\sqrt{D})K_1(\sqrt{DR_2})]} \tag{29b}$$

As can be seen, the analytical solution based on the fin approximation is much simpler as compared with the full analytical solution incorporating Brinkman and LTNE aspects.

3.6 Parameter definitions

The friction factor for forced convection in a porous annulus is defined as

$$f = \frac{2(r_2 - r_1)}{\frac{\rho_f u_m^2}{2}} \cdot \frac{dp}{dx} = \frac{8(R_2^2 - 1)P}{Re \cdot Da} \tag{30}$$

The conventional Reynolds number is defined as

$$Re = \frac{\rho_f u_m \cdot 2(r_2 - r_1)}{\mu_f} \tag{31}$$

The friction factor and the Reynolds number based on permeability are defined as:

$$f_K = \frac{\sqrt{K} dp}{\rho_f u_m^2 dx} \tag{32}$$

$$Re_K = \frac{\rho_f u_m \cdot \sqrt{K}}{\mu_f} \tag{33}$$

Thus, the dimensionless pressure drop can be expressed as

$$P = \frac{K dp}{\mu_f u_m dx} = \left(\frac{\sqrt{K} dp}{\rho_f u_m^2 dx} \right) \cdot \frac{\rho_f u_m \sqrt{K}}{\mu_f} = f_K \cdot Re_K \tag{34}$$

The Nusselt numbers at the inner and the outer walls are

$$\begin{aligned} Nu_1 &= \frac{h_1 \cdot 2(r_2 - r_1)}{k_f} = \frac{q_1}{T_{w1} - T_{fb}} \cdot \frac{2(r_2 - r_1)}{k_f} = -\frac{2\xi(R_2 - 1)}{B \cdot \theta_{f,b}} \\ Nu_2 &= \frac{h_2 \cdot 2(r_2 - r_1)}{k_f} = \frac{q_2}{T_{w2} - T_{fb}} \cdot \frac{2(r_2 - r_1)}{k_f} = -\frac{2(R_2 - 1)}{B \cdot (\theta_{w2} - \theta_{f,b})} \end{aligned} \tag{35}$$

The bulk fluid temperature can be obtained from the following integral:

$$\begin{aligned} \theta_{f,b} &= \frac{\int_A U \theta_f dA}{\int_A U dA} = \frac{1}{\pi(R_2^2 - 1)} \int_1^{R_2} \int_0^{2\pi} U \theta_f R d\varphi dR \\ &= \frac{2}{R_2^2 - 1} \int_1^{R_2} U \theta_f R dR \end{aligned} \tag{36}$$

3.7 Analysis

The dimensionless parameters defined in Eq. (6) are important for estimating the thermal performance of a porous annulus with asymmetrical heat fluxes. Due to the imposed asymmetrical heat load on the annulus, the temperature distribution will be asymmetrical. The structure of annulus will be similar to a parallel-plate channel when the outer radius becomes close to the inner radius ($R_2 \rightarrow R_1$).

The derived dimensionless velocity ($U = u/u_m$) is a function of the shape factor (s), radius ratio (R_2), and dimensionless radial position (R), which can be expressed as

$$U = F_U(s, R_2, R) \tag{37}$$

For the most complete temperature distribution for the solid and fluid (Brinkman-LTNE model), the derived dimensionless temperatures for the solid and fluid are influenced by several factors, such as $s, P, R_2, C, D, t, \xi,$ and R . This can be expressed as

$$\theta = F_\theta(s, P, R_2, C, D, t, \xi, R) \tag{38}$$

The parameters $M,$ and Da are incorporated within the shape factor (s), and expressed as

$$s = F_s(M, Da) \tag{39}$$

The dimensionless pressure drop (P) can be expressed as

$$P = \frac{K}{\mu_f u_m} \frac{dp}{dx} = \frac{f \cdot Re \cdot Da}{8(R_2^2 - 1)} = F_P(R_2, Da, fRe) \tag{40}$$

It can be seen that dimensionless pressure drop (P) is correlated with radius ratio (R_2), Darcy number (Da), and product of Reynolds number (Re) and friction factor (f).

Since thermal dispersion acts as an additional fluid heat conduction, the parameter C represents the ratio of the effective heat conduction resistance for the solid versus that for fluid, expressed as

$$C = \frac{k_{fe}}{k_{se}} = \frac{R_{se}}{R_{fe}} = \frac{\varepsilon}{1 - \varepsilon} k_r = F_C(\varepsilon, k_r) \tag{41}$$

The parameter D in Eq. (6) can be treated as the ratio of solid effective thermal resistance to local convective thermal resistance, shown as

$$D = \frac{h_{sf} a_{sf} r_1^2}{k_{se}} = \frac{r_1/k_{se}}{1/(h_{sf} a_{sf} r_1)} = \frac{R_{se}}{R_{cv}} \tag{42}$$

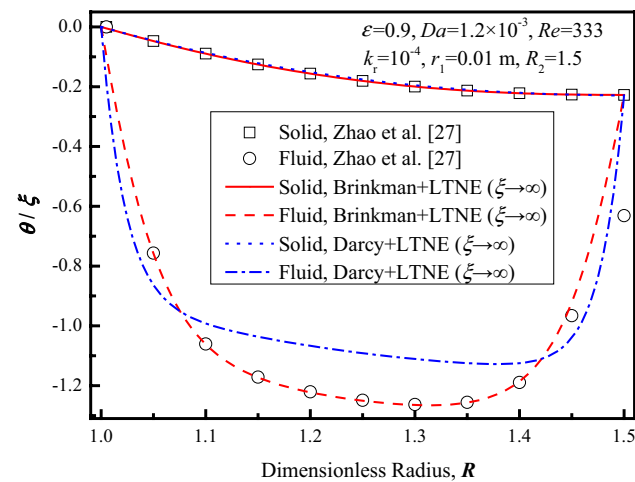


Fig. 2 Validation of the present analytical solution ($\xi \rightarrow \infty$)

The parameter t is a combination of parameters C and $D,$ and can be represented by the ratio of overall thermal resistance to the local convective thermal resistance, given as

$$t^2 = \frac{D(C + 1)}{C} = \frac{r_1/k_{fe} + r_1/k_{se}}{1/(h_{sf} a_{sf} r_1)} = \frac{R_{fe} + R_{se}}{R_{cv}} \tag{43}$$

The analytical solutions presented in this work can predict the thermal performance of convection in a porous annulus for a wide range of heat flux ratios ($\xi \in (-\infty, -R_2) \cup (-R_2, +\infty)$). The point $\xi = -R_2$ is a singular point for the present problem and the analytical values for it can be obtained when the heat flux ratio approaches this point ($\xi \rightarrow -R_2$). This singular point corresponds to two special cases for the asymmetrically heated annulus. These are

$$\xi = -R_2 \Leftrightarrow \begin{cases} \vec{q}_1 = |\vec{q}_1|, \vec{q}_2 = -\frac{|\vec{q}_1|}{R_2} \\ \vec{q}_1 = -|\vec{q}_1|, \vec{q}_2 = \frac{|\vec{q}_1|}{R_2} \end{cases} \tag{44}$$

where \vec{q}_1 and \vec{q}_2 are the heat flux vectors for the inner and outer walls respectively.

Zhao et al. [27] investigated the forced convection in an annulus filled with porous foams using Brinkman model while incorporating the thermal non-equilibrium model. In their study, the inner tube was subjected to a constant heat flux and the outer tube was adiabatic. This is a specific case when the HF ratio is infinite in the present analytical solution. Figure 2 shows a comparison of the present analytical result with the analytical result of Zhao et al. [27]. It can be seen that our analytical temperature distributions of solid and fluid are nearly the same as those obtained by Zhao et al. [27]. At the outer wall of

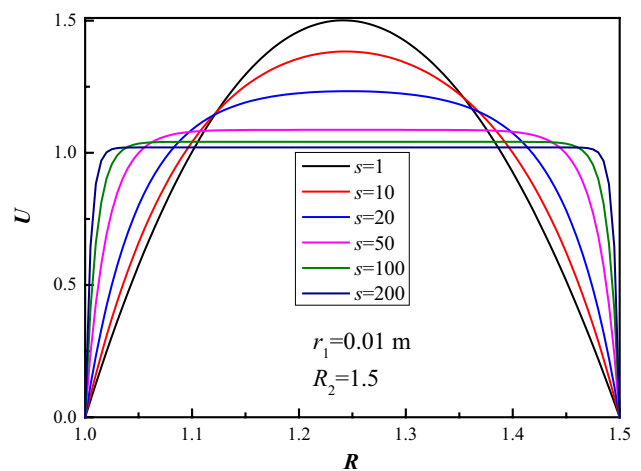


Fig. 3 Velocity profile obtained from the derived analytical solution

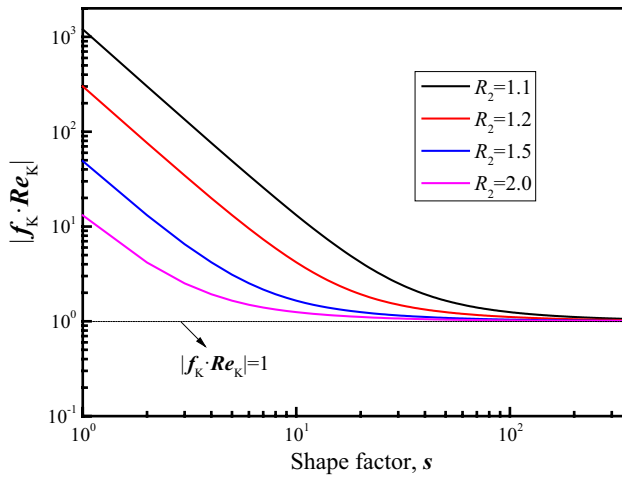


Fig. 4 Effect of the shape factor on $|f_k \cdot Re_k|$

the annulus, the fluid temperature in our solution differs slightly from that in Zhao et al. [27]. This is due to the simplified boundary condition at the outer tube leading to the following solution,

$$\frac{\partial T_s}{\partial r} = \frac{\partial T_f}{\partial r} = 0 \tag{45}$$

which is different from the present boundary condition used in Eq. (5). Comparing the Brinkman-LTNE model with the Darcy-LTE model in Fig. 2, the solid and fluid temperature of the latter model is slightly closer to the wall temperature than that of the former model. This is expected since the heat transfer obtained by using the Darcy-LTNE model is overestimated due to the uniform velocity in the Darcy model. Thus, the present analytical solution for forced convection in a porous annulus with asymmetrical heat fluxes is validated.

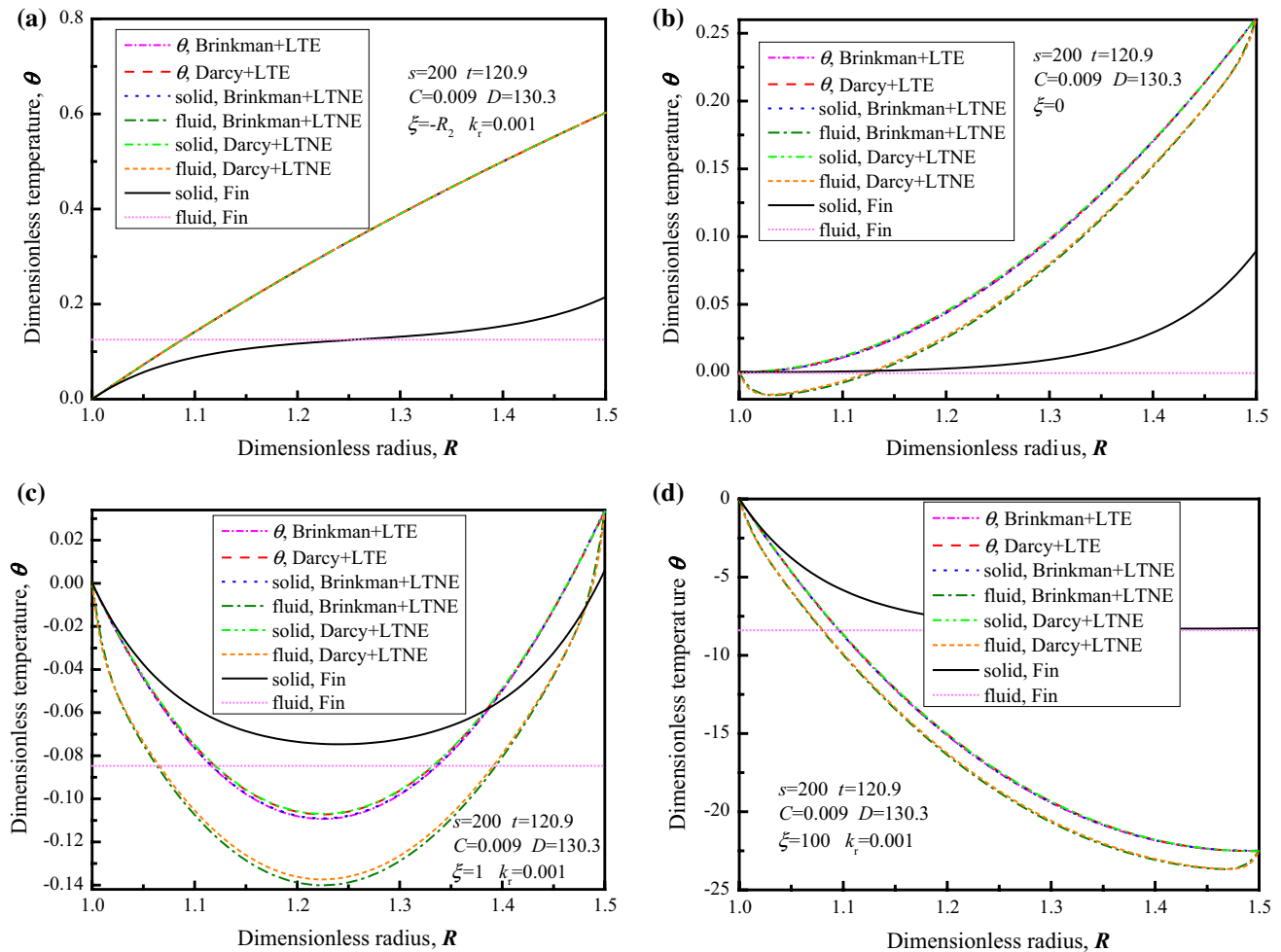


Fig. 5 Temperature profiles for different HF ratios based on the derived analytical solutions. a $\xi = -R_2$, b $\xi = 0$, c $\xi = 1$, d $\xi = 100$

4 Results and discussion

4.1 Fluid flow

In the Brinkman model, the viscous force at the solid wall is considered. As such, the velocity distribution at any cross-section is not uniform, as can be seen in Eq. (16). Figure 3 shows the dimensionless velocity profiles of the fluid flow in an annular space filled with a porous medium for different shape factors. It can be seen that an increase in the shape factor can flatten the velocity profile. The velocity profile for small shape factors is nearly parabolic and the peak velocity at the center is relatively large (1.5), which is similar with that for an open channel, while, the velocity profile for large shape factors is quite uniform and the velocity gradient near the solid wall is relatively large.

The dimensionless pressure drop equals to the product of permeability-based friction factor and

permeability-based Reynolds number, as can be seen in Eq. (34). Figure 4 shows the effect of shape factor on the absolute value of the dimensionless pressure drop (product of permeability-based friction factor and permeability-based Reynolds number) for different radius ratios. It can be seen that the absolute value of the dimensionless pressure drop decreases with an increase in the shape factor. When the shape factor is sufficiently large, the absolute value for the product of friction factor and Reynolds number based on permeability gradually approaches 1, which is the flow characteristic of the Darcy flow model [12].

4.2 Temperature profiles

Equations (9), (13), (18), (22), and (29) present the temperature solutions respectively for the Darcy-LTNE, Darcy-LTE, Brinkman-LTNE, Brinkman-LTE and the fin models.

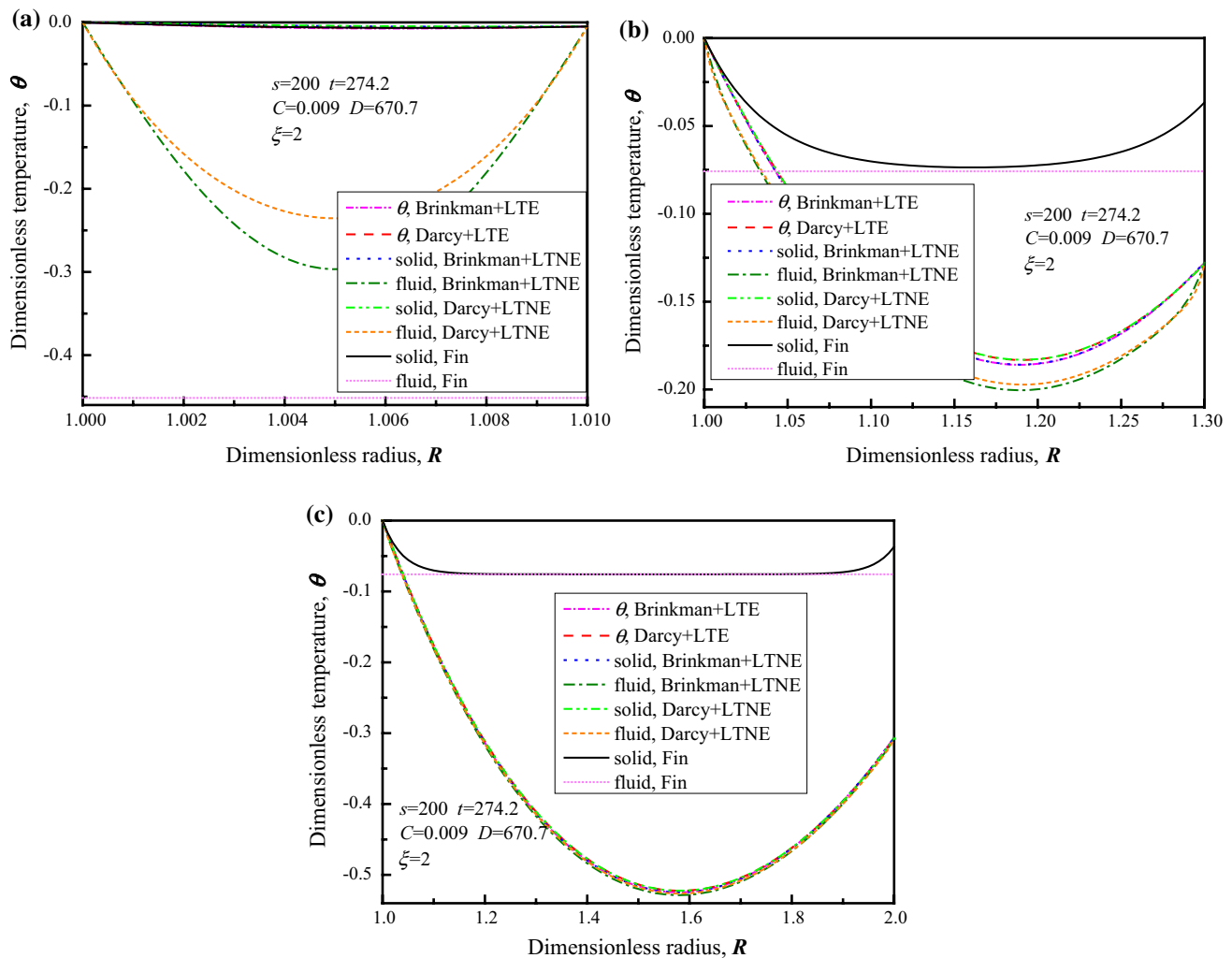


Fig. 6 Temperature profiles for different radius ratios based on the derived analytical solutions. **a** $R_2 = 1.01$, **b** $R_2 = 1.3$, **c** $R_2 = 2$

In this part, the temperature profiles for different models are analyzed and compared with each other.

Figure 5 shows the temperature profiles for the five models presented in this work for different HF ratios ($-R_2$, 0, 1, and 100). As can be seen from Eq. (44), when the heat input at one wall is equal to the heat output of the other wall, the net heat imposed on the fluid is zero. In this case, the problem shown in Fig. 1 becomes a pure heat conduction problem. Figure 5a shows the temperature profiles for different models for $\xi = -R_2$. All the temperature profiles for the solid and fluid with Darcy-LTNE, Darcy-LTE, Brinkman-LTNE, and Brinkman-LTE models are linear and coincide with each other, which is what is expected to occur when the heat conduction is the dominant heat transfer mechanism. Figure 5b shows the temperature profiles for different models for $\xi = 0$. In this case, the inner wall is adiabatic, as can be seen from Fig. 5b for all the models. Figure 5c shows the temperature profiles for different models for $\xi = 1$. Due to the geometrical asymmetry of an annular duct, the predicted temperature profiles for different models for $\xi = 1$ are also asymmetrical, which is different from asymmetrically heated parallel-plate channel [31]. Figure 5d shows the temperature profiles for different models for $\xi = 100$. In this case, the outer wall can be regarded as adiabatic compared with the inner wall. As can be seen in Fig. 5b–d, the LTE models (including Darcy-LTE and Brinkman-LTE models) always overestimate the heat transfer as compared with LTNE models (including Darcy-LTNE and Brinkman-LTNE models). Simultaneously, the fluid temperature for the Darcy models (including Darcy-LTE and Darcy-LTNE models) is slightly higher than that of Brinkman models (including Brinkman-LTE and Brinkman-LTNE models), respectively. Since the fluid temperature is assumed to be uniform in the fin model, the temperature for the fin model is quite different from those

of Darcy-LTNE, Darcy-LTE, Brinkman-LTNE, and Brinkman-LTE models.

Figure 6 shows the temperature profiles for the five analytical models at different radius ratios ($R_2 = 1.01, 1.3, \text{ and } 2$) with $\xi = 2$. Figure 6a shows the temperature profiles for the five analytical models at $R_2 = 1.01$. When the radius ratio approaches 1, the difference between inner and outer radii is small. From Fig. 6a, the temperature profiles for the solid and fluid in an annular channel for $R_2 = 1.01$ is approximately symmetrical. Figure 6b shows the temperature profiles for the five analytical models for $R_2 = 1.3$. It can be seen that the asymmetrical aspects have become more prominent. Figure 6c presents the temperature profiles for the five analytical models for $R_2 = 2$. The LTNE effect in porous media is diminished in this case due to an increase in the width of the annulus, as seen in Fig. 6c. Also as can be seen in Fig. 6, the fluid temperature for the LTE models is greater than those for the LTNE models, and the fluid temperature for the Darcy models is greater than those for the Brinkman models.

4.3 Heat transfer assessment

For the asymmetrically heated annular channel, the wall temperature at the inner surface is different from that at the outer surface. Therefore, the Nusselt numbers of the two walls sandwiching the annular channel with a porous medium are different from each other. Equation (35) defines the Nusselt numbers for the inner and outer walls and Eq. (36) presents the bulk mean temperature of the fluid. Since the effect of impermeable wall and the LTNE effect are taken into account in Brinkman-LTNE model as compared to the other models, the Brinkman-LTNE model is treated as the benchmark among the five models. In this section, the effects of the key parameters on thermal

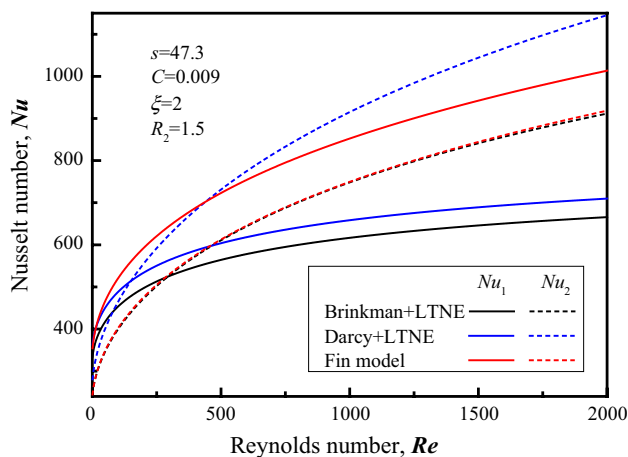


Fig. 7 Effect of the Reynolds number (Re) on the inner and outer wall Nusselt numbers

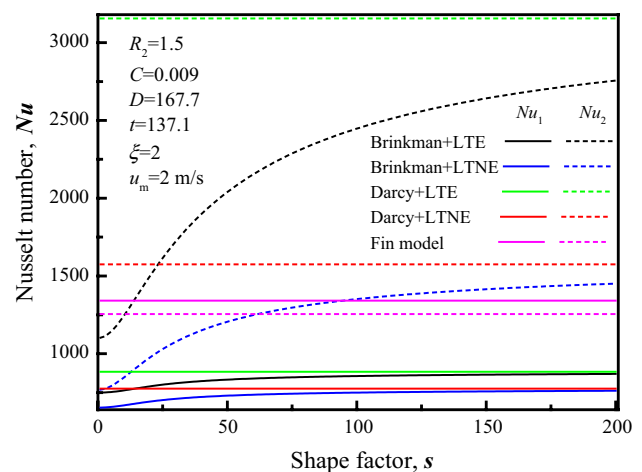


Fig. 8 Effect of the shape factor (s) on the inner and outer wall Nusselt numbers

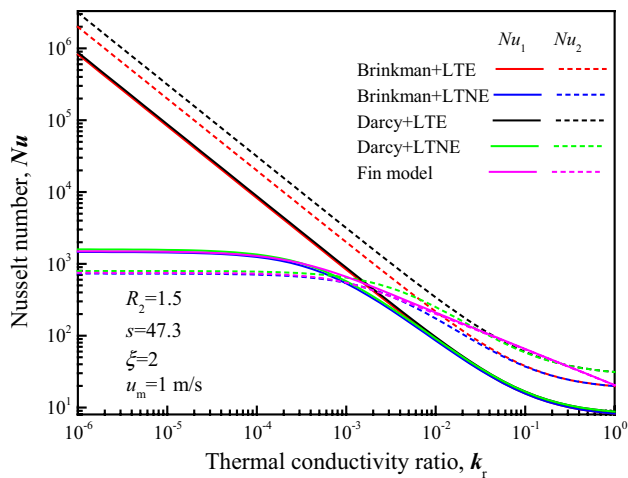


Fig. 9 Effect of the thermal conductivity ratio (k_r) on the inner and outer wall Nusselt numbers

performance of asymmetrically heated porous annulus with different models are presented and discussed.

Figure 7 shows the effect of the Reynolds number on the thermal performance of the Brinkman-LTNE, Darcy-LTNE, and the fin models. As expected, an increase in the Reynolds number increases both the inner and outer wall Nusselt numbers. The Brinkman-LTNE result is always slightly less than the Darcy-LTNE result in terms of the Nusselt numbers at the inner and outer walls. For Brinkman-LTNE and Darcy-LTNE models, since the heat flux at the inner wall is greater than that of the outer wall ($\xi = 2$), the Nusselt number at the inner wall is higher than that of the outer wall for lower Reynolds numbers. However, when the Reynolds number increases, the outer-wall Nusselt number becomes larger than the inner-wall Nusselt number. Further, the difference between the outer and inner wall Nusselt numbers increases with an increase in the Reynolds number. This is due to the larger surface area which results in a larger convective heat transfer at the outer wall. For the fin model with an assumption of uniform fluid temperature, the outer wall Nusselt number is larger than the inner wall Nusselt number, and the difference between these Nusselt numbers increases in the entire range of Reynolds numbers.

Figure 8 shows the effect of the shape factor on the thermal performance of an asymmetrically heated annulus filled with a porous medium. The shape factor including the effects of the viscosity ratio and the Darcy number, determines the velocity distribution. Thus, the analytical results for the Darcy-LTE, Darcy-LTNE, and the fin models are independent of the shape factor. As can be seen in Fig. 8, an increase in the shape factor increases the Nusselt numbers for the Brinkman-LTNE, and Brinkman-LTE models. An increased shape factor

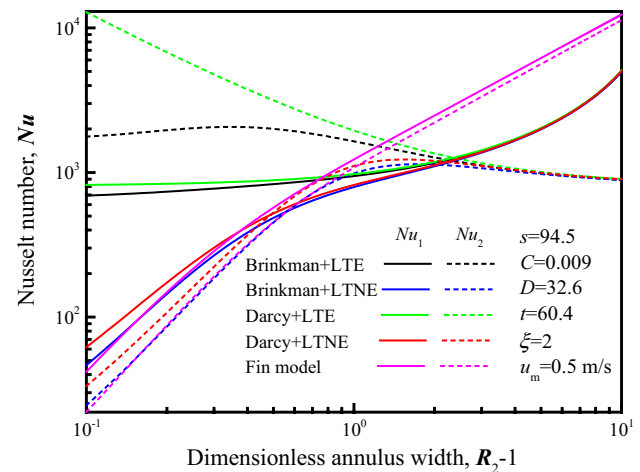


Fig. 10 Effect of the dimensionless annulus width ($R_2 - 1$) on the inner and outer wall Nusselt numbers

corresponds to a lower Darcy number, which results in a more uniform Darcy type velocity distribution. As such, as the shape factor increases, the result of the Brinkman-LTE model gradually approaches that of the Darcy-LTE model, while the result for the Brinkman-LTNE model gradually approaches that for the Darcy-LTNE model.

Figure 9 shows the effect of the thermal conductivity ratio (k_r) on the thermal performance of asymmetrically heated porous annulus predicted by the five analytical models. The comparisons between the fin model and other models show the applicable scope of the fin model for a thermal performance prediction. The increase in the thermal conductivity ratio, corresponding to a decrease in the solid thermal conductivity, leads to a lower Nusselt number at the inner and outer walls due to the weakened solid heat conduction. As seen in Fig. 9, a decrease in k_r increases the difference between LTE and LTNE results for either the Brinkman or the Darcy models. When k_r is very large ($k_r > 10^{-2}$), this difference can be neglected. However, for small k_r ($k_r < 10^{-3}$), LTNE model should be employed for the thermal performance prediction in porous media rather than the LTE model. The difference between the result for the fin model and that for the Brinkman-LTNE model is enlarged as k_r increases. In the range of $k_r > 10^{-3}$, this difference is unacceptable. When k_r is less than 10^{-4} , the results for the fin model is closer to that of the Brinkman-LTNE model than that of the Darcy-LTNE model. This indicates that the fin model is useful for predicting thermal performance of porous media for the case of very small thermal conductivity ratios. The fin model is invalid when the thermal conductivity ratio (k_r) is substantial.

Figure 10 shows the effect of the dimensionless annulus width ($R_2 - 1$) on the thermal performance of asymmetrically

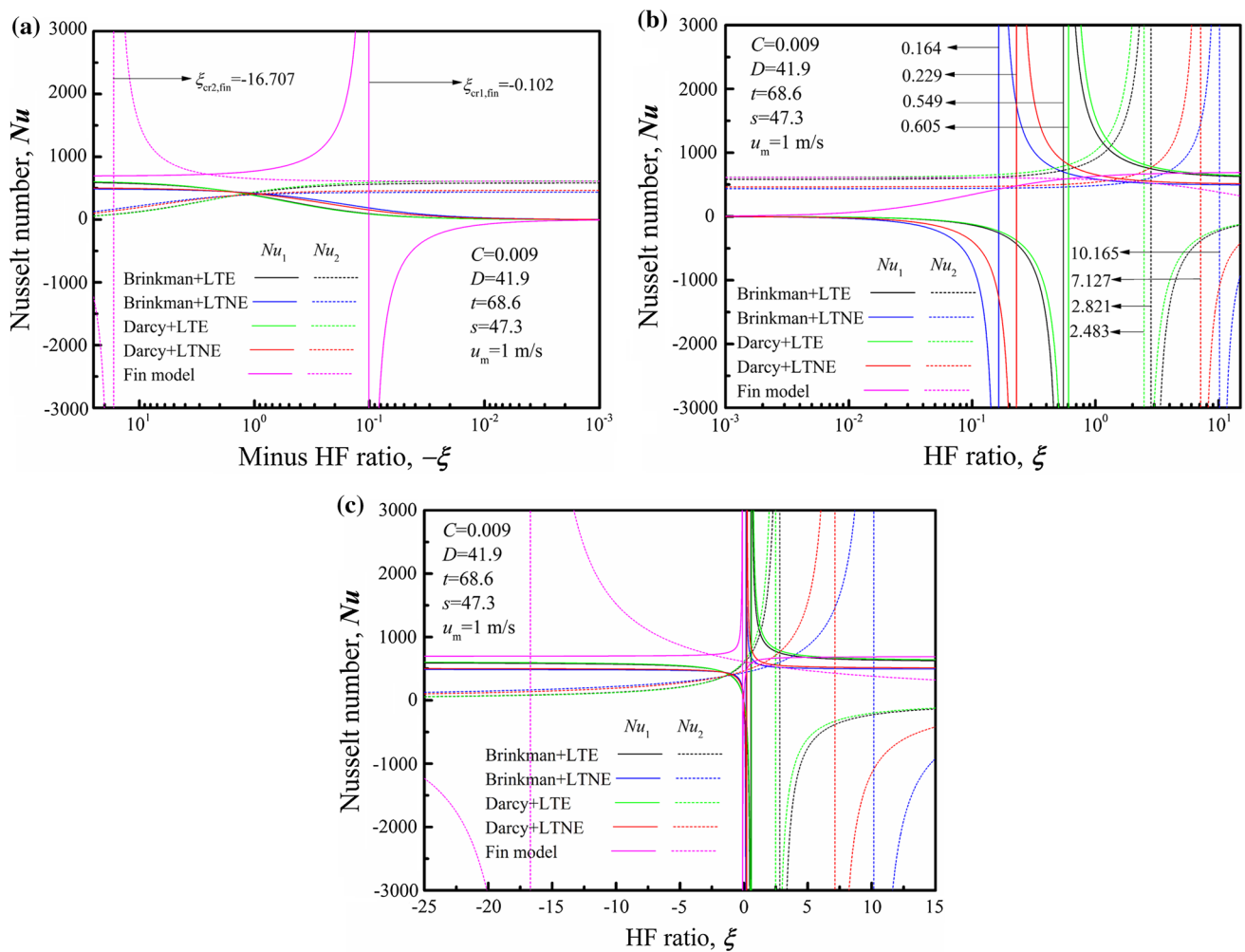


Fig. 11 Effect of the HF ratio (ξ) on the inner and outer wall Nusselt numbers. **a** $\xi < 0$, **b** $\xi > 0$, **c** overview

heated porous annulus ($\xi = 2$) for a set inner wall radius (r_1). The Nusselt numbers at the inner wall increases with an increase in the width of the annulus. An increase in the annulus width leads to a more uniform velocity distribution and relatively smaller temperature difference between solid and fluid phases. It is seen that the fin model can be applicable for a small annulus width. With an increase in the annulus width, the difference between LTE and LTNE results for either Darcy or Brinkman models decreases, and becomes negligible for $R_2 - 1 > 3$. As such, the LTE model can be applied for predicting the thermal performance of an annulus filled with a porous medium with a substantially large width.

It should be noted that when HF ratio varies, the temperature of the inner wall may equal to the fluid bulk temperature. From Eq. (35), the corresponding HF ratio for this condition, results in an infinite Nusselt number, which can be defined as the critical value of the inner wall (ξ_{cr1}). A similar feature occurs for the Nusselt number of the outer wall when its temperature becomes the same as

the fluid bulk temperature. This results in the critical HF ratio for the outer wall (ξ_{cr2}). The effect of HF ratio on predicting the thermal performance with different models is shown in Fig. 11 and the critical HF ratios for the inner and outer walls for each model can be observed in Fig. 11. Figure 11a, b are for the range of $\xi < 0$ and for that of $\xi > 0$ respectively, in logarithmic horizontal coordinate. Figure 11c shows the corresponding overview graph of Fig. 11a, b in linear horizontal coordinate. It can be seen from Fig. 11a that the critical HF ratios at the inner and the outer walls with the fin model are -0.102 and -16.707 , respectively. From Fig. 11b, the critical HF ratios at inner wall with Brinkman-LTE, Brinkman-LTNE, Darcy-LTE, and Darcy-LTNE models are approximately 0.549 , 0.164 , 0.605 , and 0.229 , respectively. While, the HF ratios at outer wall with these four models are approximately 2.281 , 10.165 , 2.483 , and 7.127 , respectively. From Fig. 11c, it can be seen that the LTE result is always greater than the corresponding LTNE result for either Brinkman or Darcy

models. The Darcy result is always larger than the corresponding Brinkman result for either LTE or LTNE models.

5 Summary

Analytical solutions for the fully-developed forced convection in a porous annulus with asymmetrical heat fluxes using five flow/thermal models are presented in this work. These analytical solutions can predict the thermal performance of an asymmetrically heated porous annulus in a wide range of radius and HF ratios. Based on the most comprehensive model, that is, Brinkman-LTNE model, it is found that the thermal performance of asymmetrically heated annulus with porous media can be improved by increasing the Reynolds number, increasing the shape factor, or decreasing the thermal conductivity ratio. An increase in the annulus width can lead to a more uniform velocity field and weakened LTNE effect in porous media. This makes the thermal performance predicted by Brinkman-LTNE model to increase first and then decrease with an increase in the width of the annulus. It is found that the LTE model always overestimates the heat transfer compared to LTNE model, and that when the thermal conductivity ratio is very large ($k_r > 10^{-2}$), the difference between LTE and LTNE results can be neglected. But the LTE model fails to predict the actual heat transfer for small thermal conductivity ratios. As expected, the Darcy model results in a larger heat transfer than the Brinkman model. The fin solution is found to provide an acceptable approximation to the Brinkman-LTNE result for low thermal conductivity ratios or small annulus widths. Overall, the LTNE phenomena is critical for thermal transport in highly conductive porous media. In addition, the viscous force near the wall has a notable effect on the global thermal performance. Thus, the analytical solution for the Brinkman-LTNE model is more accurate compared to the other simplified models and should be utilized in general. The conventional fin analysis method is generally regarded as a crude model. Finally, the critical HF ratios are found for the inner and outer walls for the five models which were analyzed in this work.

Acknowledgements This work was supported by the National Natural Science Foundation of China (51406238).

References

- Zhao F, Liu Y, Zhao X, Tan L, Geng Z (2015) Characteristics and mechanisms of solvent extraction of heavy oils from porous media. *Chem Technol Fuels Oils* 51(1):33–40
- Zhao CY (2012) Review on thermal transport in high porosity cellular metal foams with open cells. *Int J Heat Mass Transf* 55(13–14):3618–3632
- Wang F, Guan Z, Tan J, Ma L, Yan Z, Tan H (2016) Transient thermal performance response characteristics of porous-medium receiver heated by multi-dish concentrator. *Int Commun Heat Mass Transf* 75:36–41
- Hetsroni G, Gurevich M, Rozenblit R (2006) Sintered porous medium heat sink for cooling of high-power mini-devices. *Int J Heat Fluid Flow* 27(2):259–266
- Zhao CY, Lu W, Tian Y (2010) Heat transfer enhancement for thermal energy storage using metal foams embedded within phase change materials (PCMs). *Sol Energy* 84(8):1402–1412
- Wang F, Tan J, Shuai Y, Gong L, Tan H (2014) Numerical analysis of hydrogen production via methane steam reforming in porous media solar thermochemical reactor using concentrated solar irradiation as heat source. *Energy Convers Manag* 87:956–964
- Khaled ARA, Vafai K (2003) The role of porous media in modeling flow and heat transfer in biological tissues. *Int J Heat Mass Transf* 46(26):4989–5003
- Dukhan N (2013) *Metal foams: fundamentals and applications*. Destech Publications, Lancaster
- Yuan W, Tang Y, Yang XJ, Liu B, Wan ZP (2013) Manufacture, characterization and application of porous metal-fiber sintered felt used as mass-transfer controlling medium for direct methanol fuel cells. *Trans Nonferrous Met Soc China* 23(7):2085–2093
- Wen D, Ding Y (2006) Heat transfer of gas flow through a packed bed. *Chem Eng Sci* 61(11):3532–3542
- Kim T, Zhao CY, Lu TJ, Hodson HP (2004) Convective heat dissipation with lattice-frame materials. *Mech Mater* 36(8):767–780
- Nield DA, Bejan A (2013) *Convection in porous media*, 4th edn. Springer, New York
- Cheng P, Hsu CT (1986) Fully-developed, forced convective flow through an annular packed-sphere bed with wall effects. *Int J Heat Mass Transf* 29(12):1843–1853
- Vafai K, Tien HC (1989) A numerical investigation of phase change effects in porous materials. *Int J Heat Mass Transf* 32(7):1261–1277
- Chikh S, Boumedien A, Bouhadef K, Lauriat G (1995) Analytical solution of non-Darcian forced convection in an annular duct partially filled with a porous medium. *Int J Heat Mass Transf* 38(9):1543–1551
- Mitrovic J, Maletic B (2006) Effect of thermal asymmetry on laminar forced convection heat transfer in a porous annular channel. *Chem Eng Technol* 29(6):750–760
- Mitrovic J, Maletic B (2007) Heat transfer with laminar forced convection in a porous channel exposed to a thermal asymmetry. *Int J Heat Mass Transf* 50(5–6):1106–1121
- Cekmer O, Mobedi M, Ozerdem B, Pop I (2011) Fully developed forced convection heat transfer in a porous channel with asymmetric heat flux boundary conditions. *Transp Porous Media* 90(3):791–806
- Vafai K, Sozen M (1990) Analysis of energy and momentum transport for fluid flow through a porous bed. *J Heat Transf* 112(3):690–699
- Vafai K, Sozen M (1990) An investigation of a latent heat storage porous bed and condensing flow through it. *J Heat Transf* 112(4):1014–1022
- Sozen M, Vafai K (1990) Analysis of the non-thermal equilibrium condensing flow of a gas through a packed bed. *Int J Heat Mass Transf* 33(6):1247–1261
- Sozen M, Vafai K (1991) Analysis of oscillating compressible flow through a packed bed. *Int J Heat Fluid Flow* 12(2):130–136

23. Kuznetsov AV (1996) Analysis of a non-thermal equilibrium fluid flow in a concentric tube annulus filled with a porous medium. *Int Commun Heat Mass Transf* 23(7):929–938
24. Lee D-Y, Vafai K (1999) Analytical characterization and conceptual assessment of solid and fluid temperature differentials in porous media. *Int J Heat Mass Transf* 42(3):423–435
25. Xu HJ, Gong L, Zhao CY, Yang YH, Xu ZG (2015) Analytical considerations of local thermal non-equilibrium conditions for thermal transport in metal foams. *Int J Therm Sci* 95:73–87
26. Lu W, Zhao CY, Tassou SA (2006) Thermal analysis on metal-foam filled heat exchangers. Part I: metal-foam filled pipes. *Int J Heat Mass Transf* 49(15–16):2751–2761
27. Zhao CY, Lu W, Tassou SA (2006) Thermal analysis on metal-foam filled heat exchangers. Part II: tube heat exchangers. *Int J Heat Mass Transf* 49(15–16):2762–2770
28. Shaikh AW, Memon GQ (2014) Analytical and numerical solutions of fluid flow filled with and without porous media in circular pipes. *Appl Math Comput* 232:983–999
29. Ouyang XL, Vafai K, Jiang PX (2013) Analysis of thermally developing flow in porous media under local thermal non-equilibrium conditions. *Int J Heat Mass Transf* 67:768–775
30. Yang K, Vafai K (2010) Analysis of temperature gradient bifurcation in porous media: an exact solution. *Int J Heat Mass Transf* 53(19–20):4316–4325
31. Xu HJ, Zhao CY, Xu ZG (2016) Analytical considerations of slip flow and heat transfer through microfoams in mini/micro-channels with asymmetric wall heat fluxes. *Appl Therm Eng* 93:15–26